Editors' Suggestion

Epitaxial engineering of flat silver fluoride cuprate analogs

Adam Grzelak,[1,*] Haibin Su,[2,†] Xiaoping Yang,[3] Dominik Kurzydłowski,[1,4] José Lorenzana,[5,‡] and Wojciech Grochala[1,§]

[1]*University of Warsaw, Center of New Technologies, 02089 Warsaw, Poland*

[2]*Hong Kong University of Science and Technology, Department of Chemistry, Hong Kong*

[3]*Chinese Academy of Sciences, Anhui Province Key Laboratory of Condensed Matter Physics at Extreme Conditions, High Magnetic Field Laboratory, Hefei 230031, China*

[4]*Cardinal Stefan Wyszyński University in Warsaw, Faculty of Mathematics and Natural Sciences, 01938 Warsaw, Poland*

[5]*Institute for Complex Systems (ISC), Consiglio Nazionale delle Ricerche, Dipartimento di Fisica, Università di Roma "La Sapienza," 00185 Rome, Italy*

(Received 1 May 2020; accepted 14 July 2020; published 11 August 2020)

As-grown AgF_2 has an electronic structure remarkably similar to insulating cuprates, but it is extremely electronegative, which makes it hard to handle and dope. Furthermore, buckling of layers reduces magnetic interactions and enhances unwanted self-trapping lattice effects. We argue that epitaxial engineering can solve all these problems. By using a high-throughput approach and first-principle computations, we find a set of candidate substrates which can sustain the chemical aggressiveness of AgF_2 and at the same time have good lattice parameter matching for heteroepitaxy, enhancing AgF_2 magnetic and transport properties, and opening the possibility of field-effect carrier injection to achieve a unique generation of high-T_c superconductors. Assuming a magnetic mechanism and extrapolating from cuprates we predict that the superconducting critical temperature of a single layer can reach 195 K.

DOI: 10.1103/PhysRevMaterials.4.084405

I. INTRODUCTION

In recent years, silver(II) fluorides have attracted increased scientific attention because of their similarities to copper oxides, some of which are known as precursors to the most important family of high-temperature superconductors. In particular, silver(II) fluoride AgF_2 has been found to exhibit many of the same traits as one such precursor—La_2CuO_4 [1]. These traits—layered crystal structure and a charge-transfer type correlated insulating state with strong two-dimensional antiferromagnetic (AFM) coupling—are thought to be crucial for high-T_c superconductivity in cuprates, which makes AgF_2 and its derivatives a promising area of further study. Very recently Miller and Botana further highlighted the similarities between AgF_2 and oxocuprates in terms of electronic and magnetic structures [2].

It has been shown that buckling of Ag-F-Ag bonds within AgF_2 layers prevents the magnetic coupling constant (J) from reaching values as high as those found in oxocuprates and reduces the bandwidth, favoring lattice polaronic effects [1]. Indeed, in a puckered structure the out-of-plane ligand mode couples with the electronic structure to first order in displacements, while in a flat structure it couples to second order, strongly reducing polaronic effects [3].

There have been some previous experimental attempts at obtaining flat layers of AgF_2, as well as several computational studies exploring this possibility. Ternary fluoroargentates (II), such as $KAgF_3$ or Cs_2AgF_4, contain flat layers in their crystal structures, but antiferro orbital ordering accompanied by antiferrodistortive ordering of Ag-F bonds (i.e., that the bonds are alternately long and short) within any given layer precludes the emergence of two-dimensional (2D) AFM coupling [4–6] according to Goodenough-Kanamori-Anderson rules [7,8].

Initial computational studies suggested that a flat-layered AgF_2 polymorph could be stable at high pressure [9] and exhibit much enhanced superexchange interactions as compared to ambient-pressure polymorph [10]; however, subsequent x-ray diffraction studies of AgF_2 compressed up to 40 GPa and more detailed density functional theory (DFT)+U calculations have shown that AgF_2 transforms instead into a nanotubular polymorph at ca. 15 GPa [11]. Although these nanotubes lack long-range AFM ordering, interactions within constituent $[Ag_2F_7]^{3-}$ dimers via almost linear Ag-F-Ag bridges are strongly enhanced (3.5-fold) compared to ambient-pressure AgF_2, which further justifies the search for flat-layered AgF_2 systems exhibiting linear Ag-F-Ag bridges [12].

Theoretical models of an isolated layer of AgF_2 suggest that it preserves puckering typical of its condensed phase form [13]. Our proposition is to explore the possibility to stabilize a flat form of AgF_2 via epitaxial engineering. We are motivated by the enormous progress in this field in the last decades. Similar to our aim, a structure different from the bulk form of

*a.grzelak@cent.uw.edu.pl
†haibinsu@ust.hk
‡Jose.lorenzana@cnr.it
§w.grochala@cent.uw.edu.pl

CuO has been stabilized with this approach [14]. Furthermore, it has being demonstrated that using a double-layer transistor geometry it is possible to explore a sizable part of the phase diagram of a unit-cell-thick cuprate raising T_c from zero to nearly 30 K [15]. Also encouraging is the order of magnitude enhancement of T_c in FeSe on going from the bulk form to a monolayer grown on $SrTiO_3$ [16,17], the overcoming of the maximum T_c of the $La_{2-x}Sr_xCuO_4$ family at the interface between nonsuperconducting underdoped and overdoped layers [18] as well as metallicity [19] and superconductivity [15,20] appearing at the interface of insulating oxides.

AgF_2 is a commercially available compound, utilized for its strong oxidizing and fluorinating properties [21]. Indeed, recent computations of the work function of AgF_2 show that a single layer of this compound could easily take away electrons from the surface of most inorganic solids with which it comes into contact [13]. Thus, the identification of an appropriate substrate that can satisfy all epitaxial and chemical constraints is extremely challenging. In this work, we show that the list of materials that can serve as substrates or spacers is limited but not at all null and consists of certain fluorides of closed-subshell metal cations. We theoretically explore stability, as well as magnetic and electronic properties of a single flat layer of AgF_2 deposited on the most promising candidates (binary and ternary metal fluorides). Using a semiempirical approach we estimate the critical temperature. In addition, we examined a AgF_2 monolayer placed on an exemplary oxide surface (MgO) to get insight into a possible electron transfer between the reactive AgF_2 monolayer and the substrate.

II. COMPUTATIONAL METHODS

All calculations were carried out within the density functional theory (DFT) approach as implemented in VASP software [22–26], using a GGA-type Perdew-Burke-Ernzerhof functional adapted for solids (PBEsol) [27]. On-site Coulombic interactions of Ag *d* electrons were accounted for through DFT+U correction as introduced by Liechtenstein *et al.* [28], with the Hubbard U and Hund J_H parameters for Ag set to 5 and 1 eV, respectively [29]. Plane-wave cutoff energy of 520 eV was used in all systems, except for those containing lithium (650 eV). k spacing of 0.03 $Å^{-1}$ was used for all calculations. The NUPDOWN tag was used to enforce total spin in the FM state.

For all candidate substrates, we first optimized the geometry of the bulk compound in a $2 \times 2 \times 2$ supercell. In the next step, we created a vacuum slab containing several layers of the compound and relaxed atomic coordinates in the direction perpendicular to the surface (by convention referred to as z), except for three central layers. We then placed an AgF_2 monolayer on the surface and relaxed z coordinates of its atoms and the atoms in the top three layers of the substrate. As described in detail below, we found three different structures of the monolayer: corrugated orthorhombic (domain I), flat tetragonal (domain II) and quasimolecular (domain III). In selected representative cases, we also relaxed x and y coordinates in the AgF_2 monolayer to investigate possible surface reconstructions. Such process was found to occur only in domain III systems while in domains I and II atoms of AgF_2 retain their high-symmetry positions along the x and y axes.

Magnetic interactions in the AgF_2 layer were evaluated with antiferromagnetic coupling constant J_{2D} ("2D" stands for two-dimensional coupling within the monolayer), calculated using collinear configurations and the broken symmetry method as $J_{2D} = E_{AFM} - E_{FM}$, where E_{AFM} and E_{FM} are energies per silver of antiferromagnetic and ferromagnetic solutions, respectively. By this convention, J_{2D} is negative in AFM systems. In all the discussion below by "larger/smaller J_{2D}" we mean larger/smaller in magnitude. For most interesting systems, J_{2D} was additionally calculated with the HSE06 hybrid functional [30]; VESTA [31] software was used for visualization of structures, spin density maps, and electron localization function. Band structures and electronic density of states (eDOS) were plotted with P4VASP [32] software.

III. RESULTS AND DISCUSSION

Epitaxial growth of a single layer of AgF_2 on a fluoride substrate, which enforces a particular length of Ag-F-Ag bridges, represents an experimental possibility for strain stabilization of a single flat layer. Consequently, we have screened the ICSD structural database for candidate structures and selected seven known fluoride systems based on two criteria: (a) cell dimensions in the range ca. 4.0–4.2 Å, corresponding to Ag-F distance of 2.0–2.1 Å—experimental value in bulk AgF_2 is ca. 2.07 Å [33]; (b) chemical composition—no open *d*-subshell metal cations to avoid magnetism and propensity towards oxidation. These fluorides adopt either rocksalt or perovskite structure, while SnF_4 constitutes a sublattice of a classical tetragonal double-perovskite structure. We also used three hypothetical hybrid fluorides, $KZn_{0.5}Cd_{0.5}F_3$, $KZn_{0.25}Cd_{0.75}F$ and $Na_{0.25}Li_{0.75}F$, which provided more data points filling the gaps within the aforementioned Ag-F bond length range. On top of that, three systems which did not meet some of the criteria above, were selected for comparison: (a) $KCdF_3$ and $RbCdF_3$, with an even larger unit cell vector (ca. 4.4 Å) and (b) MgO (an oxide rather than a fluoride).

An example of the optimized AgF_2-on-fluoride model is presented in Fig. 1. The five F atoms form a tetragonal pyramid around each Ag atom. The distance to the apical F is in all cases larger than that to the in-layer F atoms, which can be interpreted as a manifestation of Jahn-Teller effect in a d^9 metal cation such as Ag(II). Detailed structural information on the AgF_2 monolayer on studied fluoride substrates is listed in Table I, and the structural (POSCAR) files are given in the Supplemental Material (SM) [34].

Since an isolated layer of AgF_2 has a tendency to corrugate [13], we also performed optimization of an initially corrugated structure on all fluoride surfaces listed in Table I. Overall, we can distinguish three domains in the studied range of Ag-Ag distance: I—below ca. 4.0 Å (too short), II—4.0–4.25 Å (optimum), III—above ca. 4.25 Å (too long), and the behavior of the AgF_2 layer is different in each domain. For substrates with unit cell dimensions in domain I, the orthorhombic corrugated solution is more stable. Above a certain Ag-Ag distance (ca. 4.0 Å) (domain II), the initially corrugated layer flattens out during optimization and results in virtually the same geometry as optimization of the flat layer—the Ag-F-Ag bond angle differs by no more than 0.2° in most of these cases. Depending on the substrate, we have found cases in

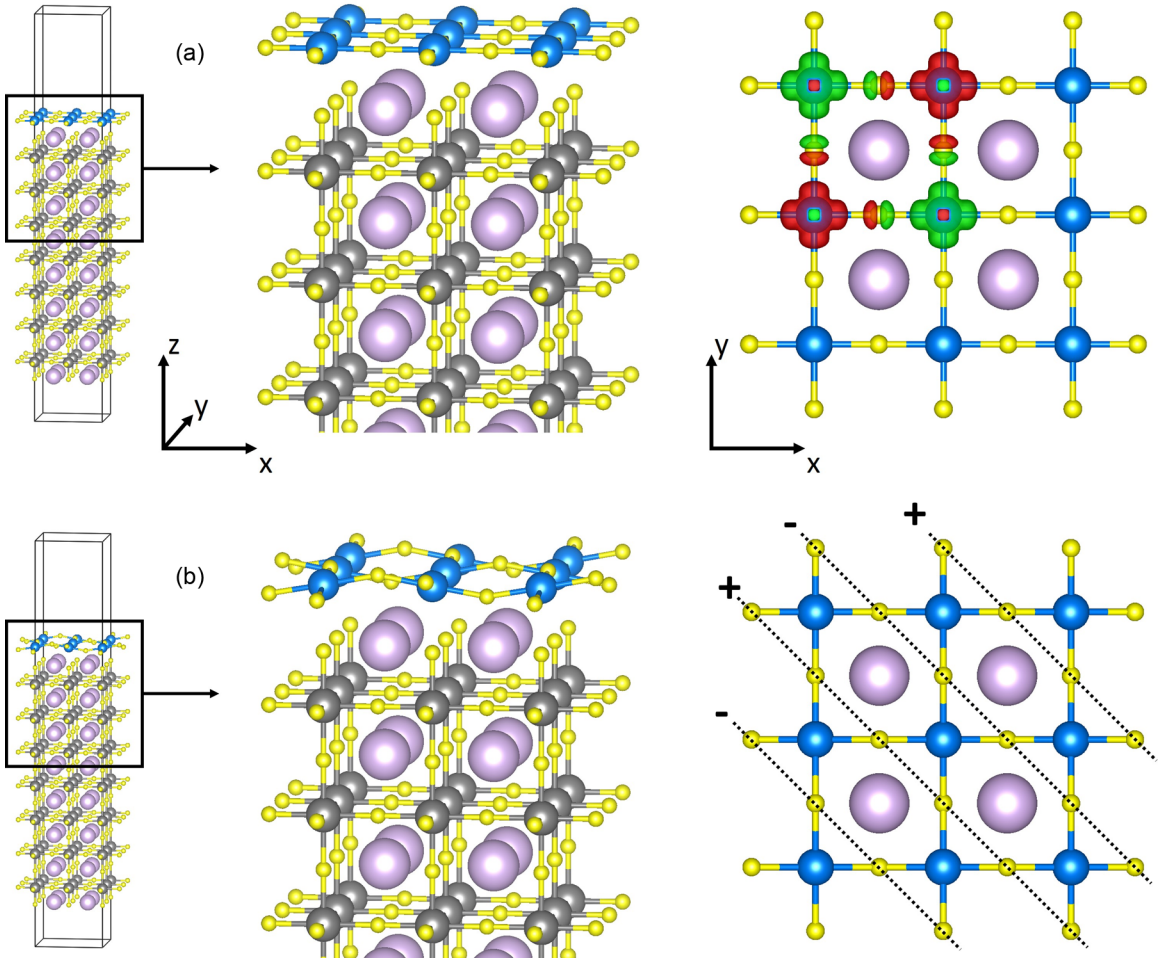

FIG. 1. AgF_2 monolayer on an example substrate ($KMgF_3$). A—tetragonal (flat); B—orthorhombic (corrugated). The "+" and "–" signs indicate z displacement of F atoms relative to Ag atoms. Left panel—view of the entire unit cell; central panel—close-up of several top layers; right panel—view along z axis. Color code: blue—Ag; yellow—F; purple—K; dark gray—Mg. Ag-F bonds between monolayer and substrate and K-F bonds are not shown for clarity. In the top right panel, we show also the magnetization density in selected sites (red and green).

which the energy gain due to corrugation of a flat layer is quite large [tens of meV per formula unit (f.u.) of AgF_2, which corresponds to several kJ mol^{-1}] and cases in which there is no tetragonal distortion. Strikingly, we have found no cases in between suggesting that the transition between the flat tetragonal (domain II) and corrugated orthorhombic (domain I) is quite abrupt. The ground state of the flat layer in domain II is an antiferromagnetic charge-transfer insulator according to the Zaanen-Sawatzky-Allen classification scheme [35], as discussed in more detail below. The magnetic moment is due to a half-filled $d(x^2\text{-}y^2)$ orbital nicely mimicking cuprates as can be seen from the shape of the magnetization density in Fig. 1.

Finally, while the AgF_2 layer in domain III is flat, as desired, yet the tetragonal arrangement (typical for domain II) is now unstable towards a surface reconstruction with symmetry lowering. Examination of the magnetization density reveals that the orbital ordering is different. Indeed, instead of the half-filled $d(x^2\text{-}y^2)$ orbital now a $d(z'^2)$ -like orbital sustains the magnetization, with z′ oriented along the planar Ag-F bond and rotating from one site to the next. Clearly the orbital order has switched to antiferro and the resulting geometry is composed of quasi-0D AgF_2 dumbbells where each Ag atom has two shorter and two longer F contacts (Fig. 2). This implies the presence of both short and long Ag-F bonds in the superexchange pathway as discussed in the SM [34].

Typically, these solutions turned out to be more stable by between 10 and 90 meV per f.u., i.e., several kJ mol^{-1} (increasing with unit cell dimensions) from the higher-symmetry solutions in the cases studied. For comparison, analogous calculations in systems in domain II ($RbMgF_3$, SnF_4, and $Na_{0.25}Li_{0.75}F$) starting from lower-symmetry quasi-0D AgF_2 molecules yielded a flat tetragonal AgF_2 monolayer with uniform Ag-F bond length, equivalent to the solution listed in Table I, indicating that systems in domain II (with Ag-Ag distance shorter than 4.3 Å) do not undergo decomposition into "molecules."

Since the energy difference between layers with flat and corrugated orientation in bulk AgF_2 (Table I) is equal to ca. 293 meV per f.u. (ca. 28 kJ mol^{-1}), one may conclude that epitaxial deposition of AgF_2 on proper substrates typical of domain II indeed has the potential of overcoming the substantial energy barrier needed for obtaining stable, flat layers of AgF_2. In addition, we investigated the nature

TABLE I. Structural and magnetic data for AgF_2 layers on fluoride substrates, calculated with PBEsol+U, listed in the order of increasing Ag-Ag distance for fluoride substrates. "f.u." stands for a formula unit of AgF_2.

	Substrate	Ag-Ag distance (Å)	Ag-F bond (Å) In layer[a]	Ag-F bond (Å) Apical	Ag-F-Ag angle (deg)	Symmetry[b]	$J_{2D}^{\text{PBEsol+U}}$ (meV)	Ag magnetic moment (μ_B)	E(g.s.)–E(flat)[c] (meV per FU)
I	$KMgF_3$	3.985	2.025	2.434	159.3	+−	−214.9	0.503	–29.6
	$AgZnF_3$	3.989	2.046	2.380	154.0	+−	−174.9	0.510	–73.7
	LiF	3.999	2.041	2.544	156.1	+−	−194.6	0.506	–59.5
II	$RbMgF_3$	4.055	2.028	2.414	178.4	++	−264.7	0.486	0.0
	$KZnF_3$	4.059	2.029	2.373	178.0	−−	−234.1	0.469	0.0
	SnF_4	4.106	2.053	2.715	179.5	++	−250.6	0.477	0.0
	$CsMgF_3$	4.177	2.089	2.460	175.2	++	−207.0	0.486	0.0
	$Na_{0.25}Li_{0.75}F$	4.217	2.109	2.391	175.8	−−	−207.8	0.479	0.0
	$KZn_{0.5}Cd_{0.5}F_3$	4.226	2.113	2.299	176.9	−−	−150.1	0.439	0.0
III	$KZn_{0.25}Cd_{0.75}F_3$	4.315	2.054	2.219	176.9	−−	−74.2	0.457	–11.5
	$KCdF_3$	4.399	2.034	2.164	177.2	−−	−49.5	0.481	–52.3
	$RbCdF_3$	4.422	2.029	2.176	179.0	−−	−55.0	0.493	–87.1
	MgO	4.210	2.117	2.410	167.8	−−	+18.2	0.182	–
	Bulk AgF_2 (tetr.)[d]	4.046	2.023	n/a	180.0	+−	−288.1	0.487	n/a
	Bulk AgF_2 (orth.)	3.736	2.070	2.569	129.0	n/a	−51.0	0.570	–292.9

[a]In domain I, the mean value of the Ag-F bond length is given; in domain III, the shorter distance (i.e., within the AgF_2 quasimolecule) is given. In domain I structures, there are two nonequivalent Ag-F-Ag angles which differ by less than 3°. We report the mean value.
[b]The sign represents the F higher (+) or lower (–) than the Ag in the uppermost layer. +− is the two-up, two-down configurations of the four F's surrounding an Ag as represented in Fig. 1(b). ++ or −− represents all F's displaced in the same direction.
[c]E(g.s.) is the energy of the lowest-energy (ground-state) configuration, E(flat) refers to the energy of the almost flat (i.e., Ag-F-Ag angle >175°) tetragonal configuration with all Ag-F bonds equal, obtained by starting from a perfectly flat AgF_2 layer. In domains I and III, the lowest-energy configurations are orthorhombic: corrugated and quasimolecular, respectively. In domain II, the solutions starting from either corrugated or quasimolecular structures lead to almost flat structure, equivalent in energy to the tetragonal solution; thus, the flat (tetragonal) solution is the ground state.
[d]Hypothetical flat polymorph of AgF_2.

of bonding between the AgF_2 monolayer and the fluoride substrate by means of electron localization function (ELF) visualization [36]. The ELF analysis indicates predominantly ionic interactions between the AgF_2 layer and the substrate; the detailed results can be found in the SM [34].

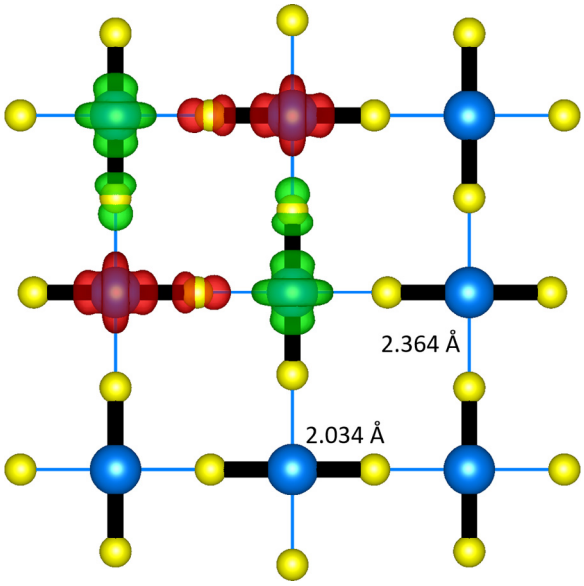

FIG. 2. Lowest-energy structure of AgF_2 monolayer on sample substrate from domain III—view along the z axis. Note the varied Ag-F distance (given for $KCdF_3$), indicating AgF_2 molecule formation. Red and green show the magnetization density in selected sites.

Flattening of the AgF_2 layers should naturally result in enhancement of the AFM interactions within the sheets. Indeed, an increase in the intensity of superexchange interactions in comparison to bulk AgF_2 is readily apparent in domains I and II (Table I). The highest value of J_{2D} (ca. –265 meV) was obtained for the $RbMgF_3$ substrate, i.e., the one with the shortest Ag-Ag distance within domain II. The J_{2D} calculated for bulk AgF_2 (with corrugated layers) using the same methodology is over fivefold smaller (–51 meV). For the promising $RbMgF_3$ system, we additionally calculated J_{2D} using the HSE06 hybrid functional [30], which yielded values of –265.2 meV—virtually identical to the PBEsol+U value. J_{2D} is also enhanced in domain I, although to a lesser extent because of buckling of the Ag-F-Ag bond, which is still substantial (150°–160°), yet less pronounced than in bulk AgF_2 (129°).

Errors in the computation of J can be estimated comparing with experimental values. Our PBEsol+U estimate for bulk AgF_2, $J_{2D} = -50$ meV, is smaller than the experimental [1] value –70 meV, which suggests that real values may be even larger, but our experience with the HSE06 functional is that it overestimates the experiment by ca. 10% in similar systems with strong AFM superexchange, such as La_2CuO_4 or $CsAgF_3$ [37]. In that case, the normalized value for J_{2D} in a $RbMgF_3$-AgF_2 surface system would be equal to ca. –240 meV. At any rate, both PBEsol+U and HSE06 results for

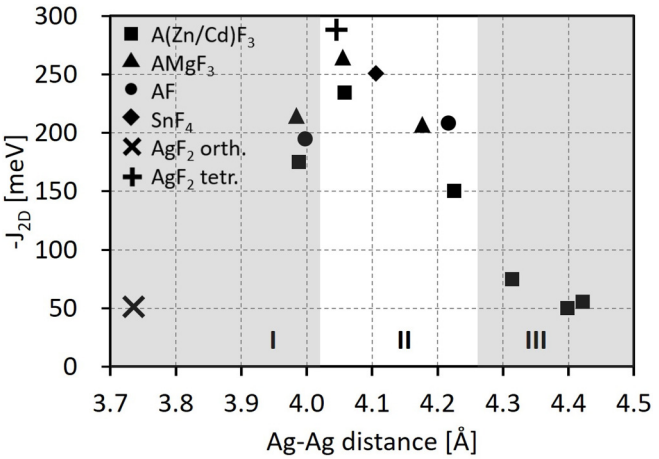

FIG. 3. Dependence of antiferromagnetic coupling constant ($-J_{2D}$) on Ag-Ag distance—on different surfaces and in bulk AgF_2. Roman numerals and shading indicate three key domains (see text). J_{2D} for bulk AgF_2, as calculated using PBEsol+U, are shown for both ground-state orthorhombic (×) and a hypothetical tetragonal structure (+). "A" in formulas stands for alkali metal cation.

our systems surpass the values in several cuprates (100–130 meV) roughly by a factor of 2.

As Table I and Fig. 3 show, J_{2D} value drops steadily with Ag-Ag distance in domain II, as could be expected, and it is substantially decreased in domain III. Since substrates in the latter range have a significantly larger lattice constant, and the Ag-F-Ag superexchange pathway involves short and long Ag-F separations, a much smaller J_{2D} in this system is unsurprising. Notice that a different type of antiferrodistortive Ag-F bond ordering leads to ferromagnetic interactions in AgF_2 layers in fluoroargentates with double-perovskite crystal structure. [5] In that case, a lobe of an active $d(x^2\text{-}y^2)$ orbital is nearly orthogonal to the basal plane of the neighbor $d(x^2\text{-}y^2)$ orbitals so that the effective hybridization tends to cancel. This is not the case here where the active orbitals have $d(z^2)$ symmetry in domain III so that nearest-neighbor active d orbitals hybridize with the same bridging p orbital (see the SM for a modeling of this effect [34]).

We were interested to see whether there exists a simple relationship between the strength of AFM interactions and the Ag-Ag distance in the monolayer (Fig. 3). As expected, J_{2D} appears to gradually decrease with the increasing distance in the studied range, but remains larger than typical cuprates (greater than 150 meV up to ca. 4.2 Å distance). A strong decrease, down to only tens of meV, is found in domain III due to the antiferro orbital ordering. These changes can be attributed to the modulation of the hybridization matrix elements among active d and p orbitals in Ag and F both due to changes in bond length, R, and Ag-F-Ag angle, α. A perturbative computation yields the dominant superexchange contribution behaving as $J_{2D} \propto \cos^2\alpha/R^{16}$. As shown in the SM [34], this expression captures qualitatively and even semiquantitatively the main trends in the material dependence of magnetic interactions [38–40].

Analysis of the three-dimensional magnetization shows that magnetic interactions are confined to the AgF_2 monolayer (see SM Fig. S2.1 for the example case of $RbMgF_3$ substrate [34]). Again, this makes the studied systems very similar to undoped oxocuprates, where strong magnetic interactions are confined to $[CuO_2]^{2-}$ layers, both for the bulk systems [41] as well as for single-layer ones [42].

In order to gain insight into electronic and magnetic properties of AgF_2 monolayer on fluoride substrate, we also calculated the electronic band structure and density of states (eDOS) for all systems, an example of which is shown in Fig. 4. The circles show the weight of the Ag $d(x^2\text{-}y^2)$ and F p orbitals parallel to the Ag-F bond. The overall appearance is remarkably similar to mean-field computations in the three-band model of cuprates (see, for example, [43]), i.e., that of a charge-transfer insulator, with the lower Hubbard band (LHB) at ca. –7.5 eV and the upper Hubbard band (UHB) at ca. 1.5 eV, while the ligand band is located between the two and centered at ca. –3 eV. The valence band, shown schematically with an orange dashed line, appears very faint because the weight is distributed over many states due to strong mixing with the substrate. The overall weight is, however, considerable as can be seen from the eDOS.

There is strong admixing between the Ag and F states just below the Fermi level, which indicates a marked covalence of Ag-F bonds [44]. The indirect band gap amounts to ca. 1 eV—less than the 1.4 eV value for the bulk AgF_2 (calculated with the same method), which helps to understand why a flat system in the absence of a rigid fluoride support has a tendency to pucker.

In addition to all fluoride systems mentioned above, we studied AgF_2 deposited on an oxide surface—MgO. Similar systems involving superlattices of ternary silver(II) fluorides and ternary titanium oxides have previously been studied [45,46]. However, there are only a few known examples of compounds in which Ag(II) atoms are coordinated by oxygen, the most important being $AgSO_4$ [47] and several fluorosulfates, e.g., $Ag(SO_3F)_2$ [48].

In fact, due to the strong electronegativity of the Ag(II) cation, all known Ag(II)-O systems can be seen as negative charge-transfer insulators (similar to some nickelates [49]). Thus, all known Ag(II)-O systems are unstable towards charge transfer (self-doping) or charge density wave (mixed valence) [21]. Figure 5 shows eDOS graphs for the AgF_2 monolayer on the MgO surface, together with eDOS for O atoms in the substrate. Although the overall structure of the Ag $d(x^2\text{-}y^2)$ part is similar to Fig. 4, the position of the UHB is shifted down to around the Fermi level and is therefore partially populated. On the other hand, the position of O p bands and their partial overlap with the UHB of Ag shows that it is partially depopulated; the aforementioned charge transfer between electron-poor Ag(II) and electron-rich O^{2-} anion takes place, resulting in an electron-doped AgF_2 layer. Doping is evident from depletion of spin on Ag atoms; for example, in a typical fluoride substrate the layer adjacent to AgF_2 one carries only minor spin contamination (ca. $0.01\mu_B$ per adjacent F atom), with the AgF_2 layer carrying null spin (with $\pm 0.49\,\mu_B$ on each Ag center); however, the spin transfer to the MgO subsurface is as large as $0.06\mu_B$, with the net spin of $0.18\mu_B$ on each Ag center of the AgF_2 layer. This implies that as much as 25% of spin is depleted from the AgF_2 layer by placing it on the MgO substrate. To quantify the degree of doping, we

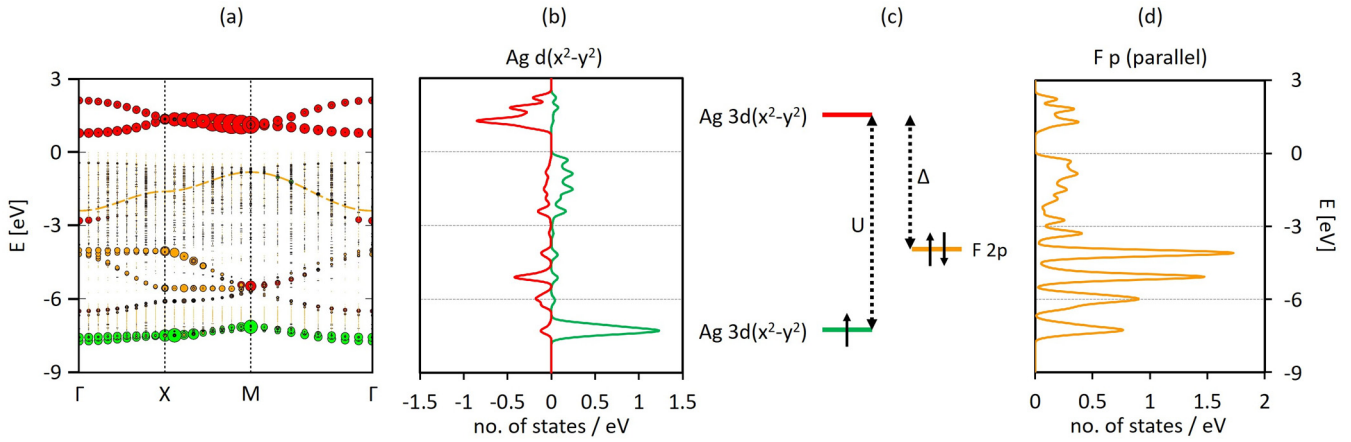

FIG. 4. (a) Band structure of AgF_2 layer on $RbMgF_3$ surface. Green (red) circles represent the character of the up (down) Ag $d(x^2\text{-}y^2)$ spin bands in an Ag with majority spin up. Orange circles represent F p character for orbitals parallel to the Ag-F-Ag bonds. The dashed orange line highlights the valence band whose spectral weight is hardly visible due to strong mixing with substrate bands. The zero of energy is placed at the highest occupied state. (b) Orbital-projected Ag $d(x^2\text{-}y^2)$ eDOS (positive up, negative down). (c) Schematic positions of levels. (d) Same as (b) for F p orbitals parallel to the bond.

compared the integrated eDOS up to E_{Fermi} (as a measure of electron count) of the AgF_2 monolayer on a substrate and the exact same monolayer (i.e., as optimized on a given substrate) isolated in vacuum. For the MgO system, we obtained the value of 0.34 excess electron per Ag atom, which is in reasonable agreement with the aforementioned distribution of spin. Comparing to the phase diagram of cuprates this corresponds to a strongly overdoped system, so superconductivity is not expected in this case. For the $RbMgF_3$ system, we obtained a value of 0.06, which suggests that even on a fluoride substrate some additional charge is transferred into AgF_2 monolayer. This, however, occurs through hybridization without adding carriers to the conduction band.

Analysis of the spin density map of the AgF_2 layer on the MgO surface (cf. SM Fig. S2.2 [34]) shows that, compared to fluoride substrates, there is much more spin density on Ag $d(z^2)$ orbitals. Conversely, nonzero spin density on O $p(z)$ orbitals indicates substantial depopulation of O states as could be expected based on previous experimental research [50].

Moreover, the AFM state of the AgF_2 monolayer on MgO becomes even less stable than the FM state; hence the positive (ferromagnetic) J_{2D} in Table I. Notice that in this case, since the system is metallic, the interpretation of J_{2D} as the interaction between localized moments loses its meaning. This reversal of the sign of the magnetic interaction suggests that doping the AgF2 layer should destroy long-range antiferromagnetic order if quantum fluctuations were taken into account beyond the present DFT method, just as for cuprates. Interestingly, ferromagnetism has recently being observed for a strongly hole-overdoped cuprate [51], similar to our theoretical finding in the case of an electron-doped cuprate analog.

The geometry of the AgF_2 layer on MgO is distorted compared to fluoride substrates of similar unit cell size (Table I): The Ag-F-Ag bridge diverges from a straight angle by over 12° due to the fact that F atoms are bound strongly by Mg(II) cations from the surface. This suggests the presence of additional strain within the monolayer, as the same phenomenon was observed for flat layers optimized on substrates in domain I.

Overall, the spin density map and eDOS graphs in Fig. 5, together with marked distortions in the monolayer, suggest

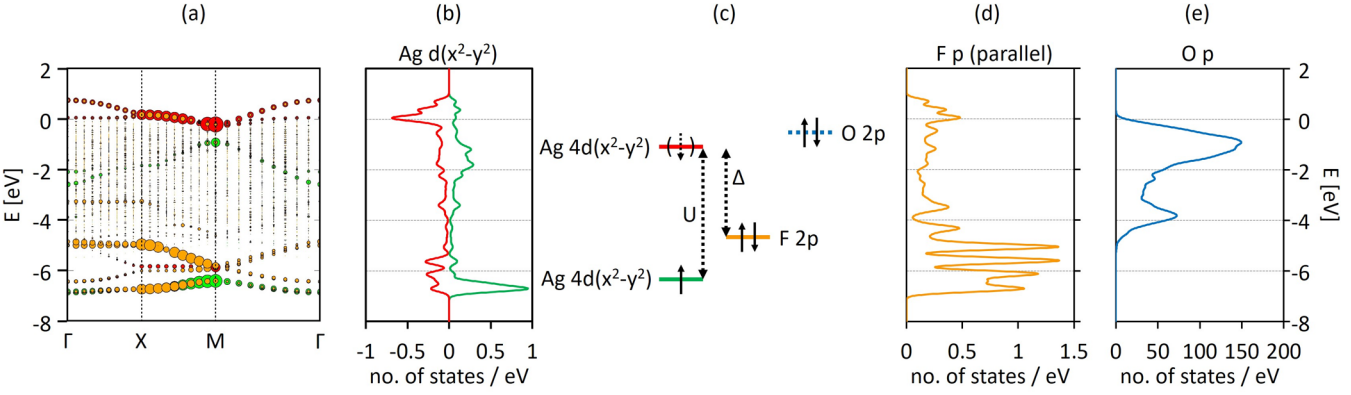

FIG. 5. Same as Fig. 4 for an AgF_2 layer on MgO surface. In panel (c) dotted arrow in brackets on the upper $4d(x^2\text{-}y^2)$ level indicates that it is partially occupied due to charge transfer from O atoms. In panel (d) we also show the O p eDOS from the substrate.

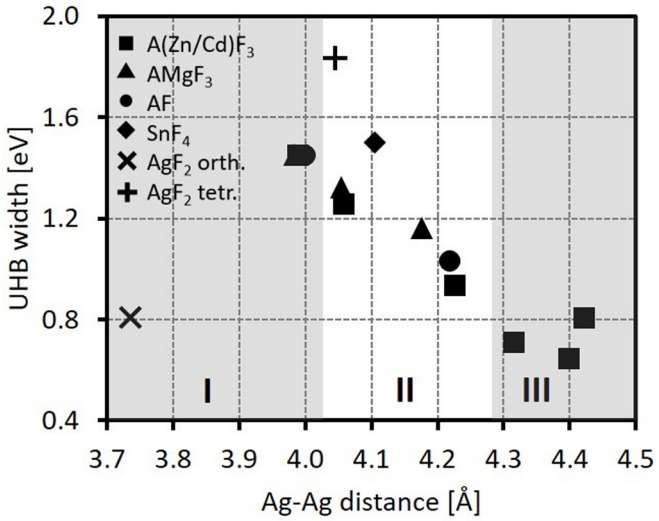

FIG. 6. Dependence of upper Hubbard band (UHB) width on Ag-Ag distance in tetragonal AgF_2 monolayer. Roman numerals and shading indicate three key domains (see text). Values for bulk AgF_2 as calculated using PBEsol+U, are shown for both ground-state orthorhombic (×) and a hypothetical tetragonal structure (+). "A" in formulas stands for alkali metal cation.

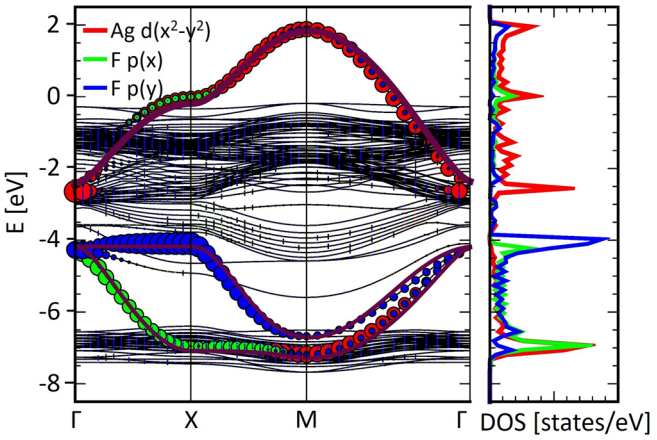

FIG. 7. Band structure of AgF_2 monolayer on a $RbMgF_3$ substrate in the nonmagnetic (metallic) solution. Circles show the character of the bands in Ag $d(x^2\text{-}y^2)$ orbitals (red) and in F $p(x)$ and $p(y)$ orbitals oriented parallel to the Ag-F bond (green and blue). The right panel shows the density of states projected on the same orbitals. Thick brown lines show the fit with a three-band tight binding model.

that deposition of the AgF_2 layer on oxide surfaces will likely result in destructive charge transfer which also affects magnetism in an undesirable way. Similar conclusions were obtained in the aforementioned computational studies of superlattices, where the AFM state was destabilized due to electronic reconstruction between AgF_2 and TiO_2 layers [45,46].

In order to explore the possibility to metallize the system by electron doping, in Fig. 6 we plotted the dependence of the width of the upper Hubbard band in the AgF_2 monolayer on the separation of Ag atoms within the monolayer. The general trend is similar as for J_{2D} since the processes for an electron to hop to an equivalent site are similar to the ones responsible for superexchange. Thus, the bandwidth increases with the reduction of interatomic distance, which is expected, given the decrease of overlap between atomic orbitals with distances as discussed in detail in the SM [34]. Widening of the UHB band in the compressed monolayers is a desired result, as it makes self-trapping (polaron formation) of additional charges less likely and facilitates metallization by electron doping of the AgF_2 monolayer. This effect adds to the reduction of linear coupling with out-of-plane ligand modes mentioned in the Introduction.

In Fig. 7 we show the band structure for $RbMgF_3$ in the nonmagnetic (metallic) solution. Most of the bands originate in the substrate (thin lines). The circles show the character of the bands in the Ag $d(x^2\text{-}y^2)$ orbitals and in the F $p(x)$ and $p(y)$ orbitals parallel to the bonds. The band structure projected on these orbitals is remarkably similar to high-temperature superconducting cuprate band structure projected on analogous orbitals of Cu and O [52–54]. The same can be said for the density of states shown in the right panel. The similarity can be further quantified by fitting the band structure with the three-band Hubbard model [53]. This model provides an excellent description of the relevant bands (Fig. 7, and SM Fig. S4.1 [34]).

As can be seen from the obtained values (Table II), the t_{pd} hopping parameter is comparable or even slightly larger than the corresponding parameter for cuprates (1.3–1.6 eV) [52,54], while the t_{pp} hopping parameter is somewhat smaller than cuprates (0.6–0.65 eV). Overall the bandwidth of the

TABLE II. Hopping parameters from the Hubbard model for AgF_2 monolayer on selected substrates. In this case we report also the hopping matrix element with an additional p orbital perpendicular to the bond (in parentheses) which needs to be considered for strong buckling. We report the nearest-neighbor hoping between Ag $d(x^2\text{-}y^2)$ and F p orbitals oriented along the bond (t_{pd}), nearest-neighbor $p(x)$ and $p(y)$ orbitals (t_{pp}), and $p(x)$-$p(x)$ and $p(y)$- $p(y)$ among next-nearer-neighbor F's bridged by Ag (t'_{pp}) .

	$RbMgF_3$ tetragonal (flat)	$KMgF_3$ tetragonal (flat)	$KMgF_3$ orthorhombic (corrugated)	Bulk AgF_2 orthorhombic (corrugated)[a]
$a_{Ag\text{-}Ag}$(Å)	4.06	3.99	3.99	3.74
t_{pd}(eV)	1.60	1.72	1.60	1.24 (0.65)
t_{pp}(eV)	0.46	0.48	0.44	0.13–0.30
t'_{pp} (eV)	0.18	0.19	0.17	

[a]Values for bulk AgF_2 are taken from Ref. [1].

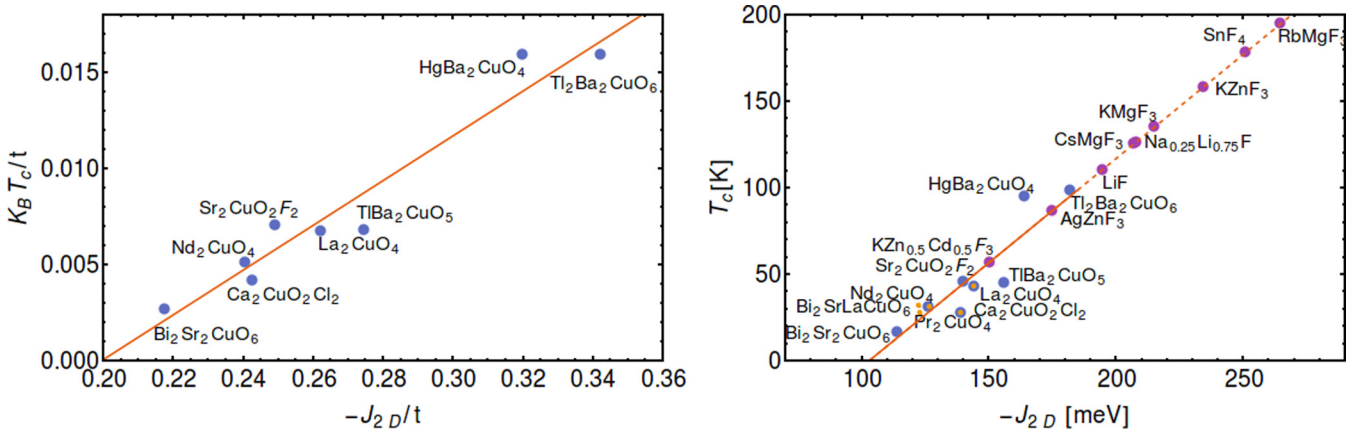

FIG. 8. Left panel: The maximum T_c value of each cuprate family (in units of t) as a function of J_{2D} in the same units. The line is the linear fit $k_BT_c/t = 0.12(\eta - \eta_c)$. Right panel: The maximum experimental T_c value of each cuprate family in Kelvin vs J_{2D} in meV for various monolayer bulk cuprates and a single AgF_2 layer labeled by the substrate. Blue dots correspond to the J_{2D} computed in Ref. [61] while small orange dots are experimental J_{2D} from two-magnon data [71–75]. Notice that for La_2CuO_4, Nd_2CuO_4, and $Ca_2CuO_2Cl_2$ both Raman and the quantum chemistry determination of J_{2D} are available. The almost perfect overlap of the points serves as a test of the accuracy of the quantum chemistry computations. The line is the linear regression over the cuprate data with slope 1.2 K meV^{-1}. The purple dots are the expected values of the maximum T_c of the AgF_2 monolayers in the different substrates.

conduction band is very similar to cuprates which will be used below.

A decrease in Ag-Ag distance from 4.06 Å in $RbMgF_3$ to 3.99 Å in $KMgF_3$ leads to a larger value of t_{pd}, but it is important to remember that this may decrease the effective hybridization as discussed in Ref. [1]. In the case of $KMgF_3$, we report in Table I and Fig. S4.1 [34] both the ground-state corrugated solution and a metastable tetragonal solution. Although the Ag-F-Ag angle is not small (159.3°), the fit with the three-band model is still quite good, in contrast with the case of bulk AgF_2 where a five-band model is needed due to the much larger bending angle (132.4°) promoting strong mixing with an additional p orbital [1]. Indeed, the band structure of the monolayer orthorhombic solution does not differ much from the tetragonal solution and the renormalization of the hopping matrix elements is modest (cf. Table II and Fig. S4.1 [34]). This suggests that also these systems may mimic cuprates providing an interesting range of electronic properties to study the effects on a possible superconducting state.

To quantify the possibilities of AgF_2 monolayers as high-T_c superconductors we first reexamine the relation between T_c and J_{2D} in cuprates; assuming a tJ-model description, the T_c/t ratio should be a function of $\eta = -J_{2D}/t$, where t is the one-band hopping. More precisely, for a two-dimensional material following the arguments of Altman and Auerbach, and Keren and collaborators [55–57] we assume that the superconducting ordering temperature should be determined by the superfluid stiffness as

$$k_BT_c = Cn_s(\eta)(-J_{2D}), \tag{1}$$

with n_s the density of superfluid pairs and C a constant of order 1. Following Ref. [55] we are assuming that the effect of J_{2D} is twofold. It provides the attraction to create bound fermion pairs [58–60] and it provides the matrix elements to make the pairs mobile. Also, within the tJ model the dimensionless superfluid density at optimum doping should be a function of η. Since bound pairs require a minimum value of η we expect that $n_s(\eta) \to 0$ below a critical ratio η_c. We therefore expand as follows: $k_BT_c/t = C\ n_s(\eta)\eta = Cn_s'(\eta_c)\eta_c(\eta - \eta_c)$. Following Moreira *et al.* [61] we restrict to bulk monolayer cuprates where layers are weakly coupled and Eq. (1) applies without the need of additional corrections due to interlayer couplings. The left panel of Fig. 8 shows that indeed there is a strong linear correlation between the maximum T_c/t of each monolayer cuprate family and η (detailed data and references can be found in the SM [34]) [62–69]. We took the t and J_{2D} values from accurate quantum chemistry computations in Ref. [61] where a similar linear relation was found with the same value of $\eta_c = 0.2$. Nicely, such value is very close to the critical value, above which bound pairs are believed to exist in the tJ model [58,60].

Notice that Moreira *et al.* considered the absolute value of T_c in Kelvin which gives a correlation almost as good as the one for dimensionless quantities considered here. This is simply because the variation of t among different families is much more modest than the variation of J_{2D}. Fitting a band with nearest-neighbor hopping to the conduction band of the paramagnetic solution of the AgF_2 monolayer on an $RbMgF_3$ we find $t = 530$ meV, again very close to typical cuprate values [61]. Thus, in first approximation, we can use common absolute units for both monolayer cuprates and silver fluorides and extrapolate from the cuprate region to the AgF_2 domain. In addition, this allows us to include cuprate materials for which quantum chemistry computations of t are not available but the experimental J_{2D} can be obtained from two-magnon Raman scattering. This is shown in the right panel of Fig. 8 where we plot the cuprate data (blue and orange points). Making a linear regression we obtain a slope of 1.2 K meV^{-1} . A similar positive correlation between T_c and J_{2D} has been found in strain engineered La_2CuO_4 [70]. It should be noted that for multilayer materials the situation is more complicated with contrasting [57,70] results beyond our scope. Using a linear extrapolation (dashed line) we obtain the

expected values of the maximum T_c attainable as a function of doping in each one of the AgF_2 monolayers (purple). We see that for the largest J_{2D} monolayer-substrate combination ($RbMgF_3$), T_c near 200 K is achievable.

IV. CONCLUSIONS

Goodenough-Kanamori-Anderson rules [7], as well as recent computational work on AgF_2 [10], provide strong indications that AFM superexchange should be strongly enhanced in flat-layered AgF_2, in particular when the Ag-F-Ag angles approach 180° [1]. Our computations indicate that a monolayer of silver(II) fluoride deposited on metal fluoride substrate has a potential for constituting a stable two-dimensional antiferromagnet, with superexchange interactions from three- to over fivefold enhanced as compared to bulk AgF_2 and simultaneously nearly twofold larger than La_2CuO_4.

There appears to be an optimal range of unit cell size of fluoride substrate, below which the deposited monolayer is prone to corrugation and above which it breaks down into molecules. Even for the corrugated monolayers the properties are much better than bulk AgF_2 with respect to the possibility to render the material metallic by doping and hopefully superconducting. In this respect, corrugation could be a helpful tool to study trends in electronic and superconducting properties as bandwidth is changed. For systems showing flat AgF_2 layers the width of the upper Hubbard band may reach 1.5 eV, which is nearly twofold larger than for bulk AgF_2 with corrugated layers.

We find that there are several compounds which can fulfill the very demanding chemical requirements imposed by AgF_2 and at the same time provide optimum heteroepitaxial conditions to create a flat monolayer. Our results clearly show that an AgF_2 layer with small buckling and not too large Ag-Ag distance exhibits oxocupratelike electronic properties both in the metallic phase and in the insulating antiferromagnetic phase. The increased width of the upper Hubbard band for flat-layer systems as compared to bulk AgF_2 (up to 1.4 eV vs 0.4 eV) [1] will likely decrease the tendency of the system for polaron localization making metallization more feasible.

Extrapolating from cuprates we argue that the maximum critical temperature of a flat AgF_2 monolayer may reach nearly 200 K, which is much larger than record multilayer cuprates (133 K) [76] Thus, our results pave the road for a family of quantum materials with very similar characteristics as high-T_c cuprates (but in the absence of copper and oxygen) which could be studied in a field-effect transistor setup [15] to provide insights on the fundamental and still mysterious physics of doped Mott insulators and high-T_c superconductors.

ACKNOWLEDGMENTS

W.G. thanks the Polish National Science Center (NCN) for support through the Maestro project (Grant No. 2017/26/A/ST5/00570). This research was carried out with the support of the Interdisciplinary Centre for Mathematical and Computational Modelling (ICM), University of Warsaw, under the ADVANCE++ grant (Grant No. GA76-19). X.Y. acknowledges the support from the National Key Research and Development Program of China (Grants No. 2018YFA0305700 and No. 2017YFA0403600), the National Natural Science Foundation of China (NSFC) (Grant No. 11674325), and support from the High Magnetic Field Laboratory of Anhui Province. J.L. acknowledges financial support from Italian MIUR through Project No. PRIN 2017Z8TS5B, and from Regione Lazio (L. R. 13/08) through the SIMAP project.

[1] J. Gawraczyński, D. Kurzydłowski, R. A. Ewings, S. Bandaru, W. Gadomski, Z. Mazej, G. Ruani, I. Bergenti, T. Jaroń, A. Ozarowski, S. Hill, P. J. Leszczyński, K. Tokár, M. Derzsi, P. Barone, K. Wohlfeld, J. Lorenzana, and W. Grochala, Proc. Natl. Acad. Sci. USA **116**, 1495 (2019).

[2] C. Miller and A. S. Botana, Phys. Rev. B **101**, 195116 (2020).

[3] M. Opel, R. Hackl, T. P. Devereaux, A. Virosztek, A. Zawadowski, A. Erb, E. Walker, H. Berger, and L. Forró, Phys. Rev. B **60**, 9836 (1999).

[4] Z. Mazej, D. Kurzydłowski, and W. Grochala, in *Photonic and Electronic Properties of Fluoride Materials*, edited by A. Tressaud, and K. Poeppelmeier, *Progress in Fluorine Science Series* (Elsevier, Amsterdam, 2016), pp. 231–260.

[5] D. Kurzydłowski, T. Jaroń, A. Ozarowski, S. Hill, Z. Jagličić, Y. Filinchuk, Z. Mazej, and W. Grochala, Inorg. Chem. **55**, 11479 (2016).

[6] S. E. McLain, M. R. Dolgos, D. A. Tennant, J. F. C. Turner, T. Barnes, T. Proffen, B. C. Sales, and R. I. Bewley, Nat. Mater. **5**, 561 (2006).

[7] J. B. Goodenough, Phys. Rev. **100**, 564 (1955).

[8] P. W. Anderson, Phys. Rev. **115**, 2 (1959).

[9] J. Romiszewski, W. Grochala, and L. Z. Stolarczyk, J. Phys.: Condens. Matter **19**, 116206 (2007).

[10] T. Jaroń and W. Grochala, Phys. Status Solidi RRL **2**, 71 (2008).

[11] A. Grzelak, J. Gawraczyński, T. Jaroń, D. Kurzydłowski, Z. Mazej, P. J. Leszczyński, V. B. Prakapenka, M. Derzsi, V. V. Struzhkin, and W. Grochala, Dalton Trans. **46**, 14742 (2017).

[12] D. Kurzydłowski, M. Derzsi, P. Barone, A. Grzelak, V. Struzhkin, J. Lorenzana, and W. Grochala, Chem. Commun. **54**, 10252 (2018).

[13] W. Wegner, K. Tokár, J. Lorenzana, M. Derzsi, and W. Grochala (2020).

[14] W. Siemons, G. Koster, D. H. A. Blank, R. H. Hammond, T. H. Geballe, and M. R. Beasley, Phys. Rev. B **79**, 195122 (2009).

[15] A. T. Bollinger, G. Dubuis, J. Yoon, D. Pavuna, J. Misewich, and I. BoŽović, Nature **472**, 458 (2011).

[16] Q.-Y. Wang, Z. Li, W.-H. Zhang, Z.-C. Zhang, J.-S. Zhang, W. Li, H. Ding, Y.-B. Ou, P. Deng, K. Chang, J. Wen, C.-L. Song, K. He, J.-F. Jia, S.-H. Ji, Y.-Y. Wang, L.-L. Wang, X. Chen, X.-C. Ma, and Q.-K. Xue, Chin. Phys. Lett. **29**, 037402 (2012).

[17] J.-F. Ge, Z.-L. Liu, C. Liu, C.-L. Gao, D. Qian, Q.-K. Xue, Y. Liu, and J.-F. Jia, Nat. Mater. **14**, 285 (2015).

[18] A. Gozar, G. Logvenov, L. F. Kourkoutis, A. T. Bollinger, L. A. Giannuzzi, D. A. Muller, and I. Bozovic, Nature **455**, 782 (2008).

[19] A. Ohtomo and H. Y. Hwang, Nature **427**, 423 (2004).

[20] N. Reyren, S. Thiel, A. D. Caviglia, L. Fitting Kourkoutis, G. Hammerl, C. Richter, C. W. Schneider, T. Kopp, A. S. Rüetschi, D. Jaccard, M. Gabay, D. A. Muller, J. M. Triscone, and J. Mannhart, Science **317**, 1196 (2007).

[21] W. Grochala, J. Supercond. Novel Magn. **31**, 737 (2018).

[22] G. Kresse and J. Hafner, Phys. Rev. B **47**, 558 (1993).

[23] G. Kresse and J. Hafner, Phys. Rev. B **49**, 14251 (1994).

[24] G. Kresse and J. Furthmüller, Comput. Mater. Sci. **6**, 15 (1996).

[25] G. Kresse and J. Furthmüller, Phys. Rev. B **54**, 11169 (1996).

[26] G. Kresse and D. Joubert, Phys. Rev. B **59**, 1758 (1999).

[27] J. P. Perdew, A. Ruzsinszky, G. I. Csonka, O. A. Vydrov, G. E. Scuseria, L. A. Constantin, X. Zhou, and K. Burke, Phys. Rev. Lett. **100**, 136406 (2008).

[28] A. I. Liechtenstein, V. I. Anisimov, and J. Zaanen, Phys. Rev. B **52**, R5467 (1995).

[29] D. Kasinathan, A. B. Kyker, and D. J. Singh, Phys. Rev. B **73**, 214420 (2006).

[30] A. V. Krukau, O. A. Vydrov, A. F. Izmaylov, and G. E. Scuseria, J. Chem. Phys. **125**, 224106 (2006).

[31] K. Momma and F. Izumi, J. Appl. Crystallogr. **44**, 1272 (2011).

[32] O. Dubay, p4vasp.at.

[33] P. Fischer, G. Roult, and D. Schwarzenbach, J. Phys. Chem. Solids **32**, 1641 (1971).

[34] See Supplemental Material at http://link.aps.org/supplemental/10.1103/PhysRevMaterials.4.084405 for complementary figures, graphs, and description of magnetic models.

[35] J. Zaanen, G. A. Sawatzky, and J. W. Allen, Phys. Rev. Lett. **55**, 418 (1985).

[36] B. Silvi and A. Savin, Nature **371**, 683 (1994).

[37] D. Kurzydłowski and W. Grochala, Angew. Chem., Int. Ed. **56**, 10114 (2017).

[38] J. C. Slater and G. F. Koster, Phys. Rev. **94**, 1498 (1954).

[39] O. K. Andersen, W. Klose, and H. Nohl, Phys. Rev. B **17**, 1209 (1978).

[40] H. Eskes and J. H. Jefferson, Phys. Rev. B **48**, 9788 (1993).

[41] M. A. Kastner, R. J. Birgeneau, G. Shirane, and Y. Endoh, Rev. Mod. Phys. **70**, 897 (1998).

[42] Y. Y. Peng, G. Dellea, M. Minola, M. Conni, A. Amorese, D. Di Castro, G. M. De Luca, K. Kummer, M. Salluzzo, X. Sun, X. J. Zhou, G. Balestrino, M. Le Tacon, B. Keimer, L. Braicovich, N. B. Brookes, and G. Ghiringhelli, Nat. Phys. **13**, 1201 (2017).

[43] Z.-H. Cui, C. Sun, U. Ray, B.-X. Zheng, Q. Sun, and G. K.-L. Chan, arXiv:2001.04951 [cond-mat.str-el] (2020).

[44] W. Grochala, R. G. Egdell, P. P. Edwards, Z. Mazej, and B. Žemva, ChemPhysChem **4**, 997 (2003).

[45] X. Yang and H. Su, Sci. Rep. **5**, 15849 (2015).

[46] X. Yang and H. Su, Sci. Rep. **4**, 5420 (2014).

[47] P. J. Malinowski, M. Derzsi, Z. Mazej, Z. Jagličić, B. Gaweł, W. Łasocha, and W. Grochala, Angew. Chem., Int. Ed. **49**, 1683 (2010).

[48] P. Leung and F. Aubke, Inorg. Chem. **17**, 1765 (1978).

[49] V. Bisogni, S. Catalano, R. J. Green, M. Gibert, R. Scherwitzl, Y. Huang, V. N. Strocov, P. Zubko, S. Balandeh, J.-M. Triscone, G. Sawatzky, and T. Schmitt, Nat. Commun. **7**, 13017 (2016).

[50] P. Malinowski, Z. Mazej, and W. Grochala, Z. Anorg. Allg. Chem. **634**, 2608 (2008).

[51] T. Sarkar, D. S. Wei, J. Zhang, N. R. Poniatowski, P. R. Mandal, A. Kapitulnik, and R. L. Greene, Science **368**, 532 (2020).

[52] O. K. Andersen, A. I. Liechtenstein, O. Jepsen, and F. Paulsen, J. Phys. Chem. Solids **56**, 1573 (1995).

[53] V. J. Emery, Phys. Rev. Lett. **58**, 2794 (1987).

[54] A. K. McMahan, J. F. Annett, and R. M. Martin, Phys. Rev. B **42**, 6268 (1990).

[55] E. Altman and A. Auerbach, Phys. Rev. B **65**, 104508 (2002).

[56] A. Keren, A. Kanigel, J. S. Lord, and A. Amato, Solid State Commun. **126**, 39 (2003).

[57] R. Ofer, G. Bazalitsky, A. Kanigel, A. Keren, A. Auerbach, J. S. Lord, and A. Amato, Phys. Rev. B **74**, 220508(R) (2006).

[58] M. Boninsegni and E. Manousakis, Phys. Rev. B **47**, 11897 (1993).

[59] P. Prelovšek and I. Sega, Phys. Rev. B **49**, 15241 (1994).

[60] F. Mezzacapo, A. Angelone, and G. Pupillo, Phys. Rev. B **94**, 155120 (2016).

[61] I. D. P. R. Moreira, D. Muñoz, F. Illas, C. De Graaf, and M. A. Garcia-Bach, Chem. Phys. Lett. **345**, 183 (2001).

[62] T. Hirayama, M. Nakagawa, A. Sumiyama, and Y. Oda, Phys. Rev. B **58**, 5856 (1998).

[63] B. Morosin, E. L. Venturini, J. E. Schirber, R. G. Dunn, and P. P. Newcomer, Phys. C (Amsterdam, Neth.) **241**, 181 (1995).

[64] Y. Kohsaka, M. Azuma, I. Yamada, T. Sasagawa, T. Hanaguri, M. Takano, and H. Takagi, J. Am. Chem. Soc. **124**, 12275 (2002).

[65] A. K. Rajarajan, A. Sundaresan, R. Kumar, M. Sharon, L. C. Gupta, and R. Vijayaraghavan, J. Phys.: Condens. Matter **4**, 6971 (1992).

[66] G. F. Sun, Y. Xin, D. F. Lu, K. W. Wong, Y. Zhang, and J. G. Stevens, Solid State Commun. **101**, 849 (1997).

[67] N. Barišić, Y. Li, X. Zhao, Y. C. Cho, G. Chabot-Couture, G. Yu, and M. Greven, Phys. Rev. B **78**, 054518 (2008).

[68] F. Jean, D. Colson, G. Collin, N. Blanchard, D. Colson, Z. Konstantinović, G. Le Bras, A. Forget, and M. Andrieux, Phys. Rev. B **68**, 174511 (2003).

[69] O. Matsumoto, A. Utsuki, A. Tsukada, H. Yamamoto, T. Manabe, and M. Naito, Phys. Rev. B **79**, 100508(R) (2009).

[70] O. Ivashko, M. Horio, W. Wan, N. B. Christensen, D. E. McNally, E. Paris, Y. Tseng, N. E. Shaik, H. M. Rønnow, H. I. Wei, C. Adamo, C. Lichtensteiger, M. Gibert, M. R. Beasley, K. M. Shen, J. M. Tomczak, T. Schmitt, and J. Chang, Nat. Commun. **10**, 786 (2019).

[71] N. Chelwani, A. Baum, T. Böhm, M. Opel, F. Venturini, L. Tassini, A. Erb, H. Berger, L. Forró, and R. Hackl, Phys. Rev. B **97**, 024407 (2018).

[72] Y. Tokura, S. Koshihara, T. Arima, H. Takagi, S. Ishibashi, T. Ido, and S. Uchida, Phys. Rev. B **41**, 11657 (1990).

[73] S. Sugai, M. Sato, T. Kobayashi, J. Akimitsu, T. Ito, H. Takagi, S. Uchida, S. Hosoya, T. Kajitani, and T. Fukuda, Phys. Rev. B **42**, 1045 (1990).

[74] S. Sugai, H. Suzuki, Y. Takayanagi, T. Hosokawa, and N. Hayamizu, Phys. Rev. B **68**, 184504 (2003).

[75] B. W. Lebert, Ph.D. thesis, Sorbonne Université, 2018.

[76] A. Schilling, M. Cantoni, J. D. Guo, and H. R. Ott, Nature **363**, 56 (1993).